NANO LETTERS

2004
Vol. 4, No. 4
569−572

Direct Observation of Nanoscale Switching Centers in Metal/Molecule/Metal Structures

Chun Ning Lau,[†] Duncan R. Stewart,[†] R. Stanley Williams,*[,†] and Marc Bockrath*[,‡]

Hewlett-Packard Laboratories, Palo Alto, California 94304 and Department of Applied Physics, California Institute of Technology, Pasadena, California 91101

Received December 2, 2003; Revised Manuscript Received February 4, 2004

ABSTRACT

Conductance switching in metal/molecule/metal structures has attracted tremendous and broad interest. Understanding the switching mechanism, which remained controversial to date, will be vital for engineering nanoscale switches crucial for memory and logic applications. Here we describe a new switching mechanism revealed by a novel scanned-probe technique that images the mechano-electrical response of a Pt/stearic acid/Ti structure switch device. In each image a single switching center, characterized by a nanoscale conductance peak, appeared or disappeared when the device was switched "on" or "off". Our results strongly indicate that the formation and dissolution of individual nanoscale filaments through the molecular layer give rise to conductance switching in our molecular structures with unusually high on/off ratios (~10^5).

Molecule-based electronic switches have attracted significant interest in recent years because of their potential applications in electronic devices, such as nanoscale memory elements or configurable logic gates. This switching behavior has been observed in a number of systems, including molecular monolayers probed by scanning tunneling microscopy (STM),[1−4] transport experiments on nanopores,[5,6] and planar cross-bar devices,[7−10] incorporating such diverse species as alkanes,[10] rotaxanes,[7,8] catananes,[11] and phenylene-ethynylene oligomers.[2,3,12,13] Various proposals have been put forward to account for the observed switching behavior, including molecular conformational change,[3,13] bond fluctuation between the molecules and their electrical contacts,[1] and electrical charge transfer.[5,14] Despite these recent efforts, however, the origin of molecular switching remains controversial.

In this letter we report a previously unobserved switching mechanism in molecular structures. We developed a novel scanned-probe technique that uniquely combined the local mechanical perturbation of metal/molecule/metal crossbar devices with electrical transport measurements. When a device was switched to high conductance state, the scanned probe image was characterized by the appearance of a single nanoscale conductance peak, which disappeared when the device was switched to low conductance state. The quantitative agreement between our results and a simple model indicates that the formation and dissolution of individual nanoscale conducting filaments through the molecular layer gives rise to the conductance switching in our, and possibly other, molecular structures.

The system we choose to investigate is Pt/stearic acid (C_{18})/Ti (Pt/C_{18}/Ti) crossbar molecular structures, consisting of planar Pt and Ti electrodes sandwiching a monolayer of 2.6-nm-long stearic acid ($C_{18}H_{36}OH$) molecules (Figure 1 inset). Electrical characterization was performed by applying a bias voltage V_b relative to the Ti electrodes. The current−voltage ($I-V$) characteristics of the as-fabricated samples were nonlinear, with zero-bias resistance typically $>10^5\ \Omega$. The devices can be switched *reversibly* and repeatedly to higher ("on") or lower ("off") conductance states by applying sufficiently large $V_b < 0$ or $V_b > 0$, respectively[10] (Figure 1). Similar switching behavior was found for other junctions with asymmetric electrodes such as Ti and Al, and for different types of molecules.[8] Interestingly, reversible switching was never observed in symmetric Pt/C_{18}/Pt devices.

Switching in our junctions is unlikely to be caused by molecular conformational change or electrical charge transfer, because stearic acid lacks redox centers, mobile subgroups, or charge reception sites. To gain further insight into the switching mechanism, we explored the mechanical and electrical properties of the Pt/C_{18}/Ti structure by using an AFM tip to scan the junction with a localized force $F_{tip} \sim 0.8\ \mu$N, while simultaneously measuring the current through the molecular junction biased at $V_b = 0.1$ V (Figure 2A). In contrast with other conducting AFM measurement,[4,15] the tip was not electrically connected to the device and acted only as a mechanical force applicator.

The pressure exerted by the tip on the junction locally depresses the Pt/C_{18}/Ti structure, compressing the molecular

* Corresponding authors. E-mail: stan.williams@hp.com; mwb@caltech.edu.
[†] Hewlett-Packard Laboratories.
[‡] California Institute of Technology.

10.1021/nl035117a CCC: $27.50
Published on Web 03/10/2004

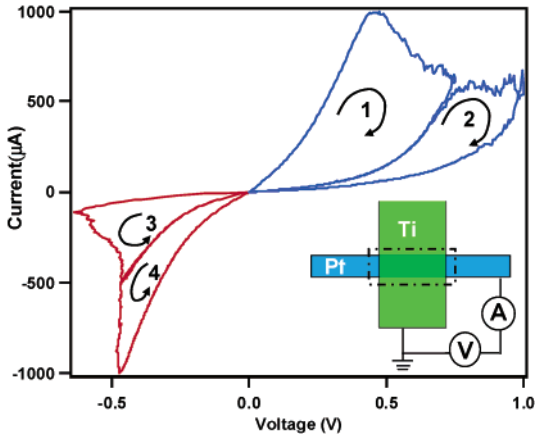

Figure 1. Current−voltage ($I-V$) characteristics showing the reversible switching cycle of the device. The arrows indicate $I-V$ sweep direction; the numbers indicate the order by which the switching was performed. A negative bias switches the device to a high conductance state (red curve), while a positive bias switches it to a low conductance state (blue curve). (inset) Schematic top view of a device, which consists of a monolayer of stearic acid molecules sandwiched between a Pt bottom electrode (blue) and a Ti top electrode (green). The dotted lines outline the AFM scan area of Figure 2B. The bottom Pt electrodes, 250 nm in thickness and 1−5 μm in width, were fabricated by standard photolithography and cleaned by oxygen RIE plasma etching. The organic monolayer was assembled on the substrate by the Langmuir−Blodgett (LB) process from a 10^{-3} M cadmium chloride solution. A 5 nm layer of Ti and a 15−25 nm capping layer of Pt were subsequently deposited through a shadow mask to form the top electrodes with width 8−18 μm.

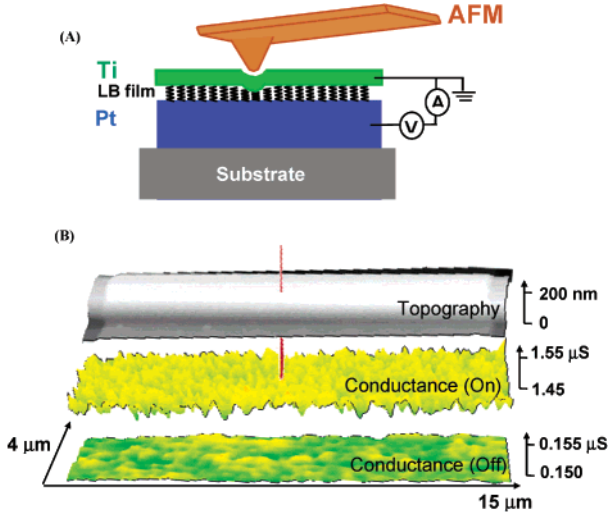

Figure 2. (A) Experimental setup (side view). The device is biased at 0.1 V and the current through the junction is measured, while a scanning AFM tip is used to produce local mechanical modulation by applying a force of 0.8 μN. (B) The topographical (top) and conductance images of a junction. The conductance map is obtained by plotting the conductance G of the junction (vertical axis) as a function of tip position (horizontal axes), representing the junction's electrical response to local mechanical pressure. The conductance and topographical maps of a junction were acquired simultaneously, so any feature in the conductance image can be located by reference to the sample topography. The AFM scan area is indicated by the dotted lines in Figure 1 inset. The conductance is relatively uniform across the junction when the junction is in the "off" state (bottom image). When switched "on" (middle), a peak in conductance emerges, which appears as the red spike piercing the top image. The peak is localized to an area ~40 nm in diameter.

layer by an amount depending on the elastic properties of the component materials. Reported values of Young's modulus E for alkanes range from 10 to 100 GPa,[15−18] on the same order of magnitude as the metals (~80 GPa). Thus, we estimate the effect of the tip by approximating the junction as a uniform half-infinite elastic medium with $E \sim$ 80 GPa. According to standard texts,[19] the local compressive strain u_{zz} at a depth d inside an elastic medium under a force F applied at a point at $x,y,z = 0$ is approximately

$$u_{zz} \sim \frac{3}{2\pi E} \frac{d^3}{(x^2 + y^2 + d^2)^{5/2}} F \qquad (1)$$

where x, y are the lateral coordinates of the point under consideration. This shows that the compression due to a point force will be distributed over a region of characteristic lateral dimension d. For our experiment probing the mechanical response of the $Pt/C_{18}/Ti$ structure, d is assumed to be the thickness of the top electrode. Thus, the spatial resolution of our technique is set by the thickness of the top electrode and the finite size of the AFM tip. Finally, using typical values of $E = 80$ GPa, $d = 30$ nm, $F = 0.8$ μN, eq 1 yields u_{zz} (0,0) ~ 0.6% or an estimated maximum monolayer compression of ~0.2 Å.

We now examine our experimental data (Figure 2B). The top image displays the device's topography, and the bottom two images its conductance $G = I/V_b$ versus the tip position, which shows the device's electrical response to the local pressure perturbation produced by the tip. Before any switching was performed on the junction, the conductance image was relatively uniform across the scan region, including both the electrodes and adjacent substrate areas (Figure 2B, bottom image). This indicates that the junction conductance exhibited no observable response to the tip perturbation. Remarkably, after the junction was switched to the "on" state, a *local* increase in G emerged when the tip pressurized a particular spot, leading to a conductance peak (middle image) with spatial dimension ~40 nm (fwhm). This indicates that the size of a "switching center", i.e., the mechanically sensitive region of the junction, is <40 nm.

Similar measurements have been performed on a total of 10 devices, and a switch to the "on" state of the $Pt/C_{18}/Ti$ structures was always accompanied by the emergence of one (and very occasionally two) new nanoscale conductance peaks, or switching centers. This is illustrated by Figure 3, which displays the $I-V$ characteristics of two different devices in their "off" (blue) and "on" (red) states. For device A, the zero-bias conductances G_0 are 0.17 μS ("off" state) and 1.45 μS ("on"); for device B, $G_0 \sim 7$ nS and ~ 770 μS, respectively. Despite the large variation of G and on/off ratios exhibited by the two devices, their behavior is qualitatively similar: in the "off" state of each device the conductance map was uniform across the junction, while in the "on" state both devices were characterized by the emergence of a single switching center in response to pressure (Figure 3, insets).

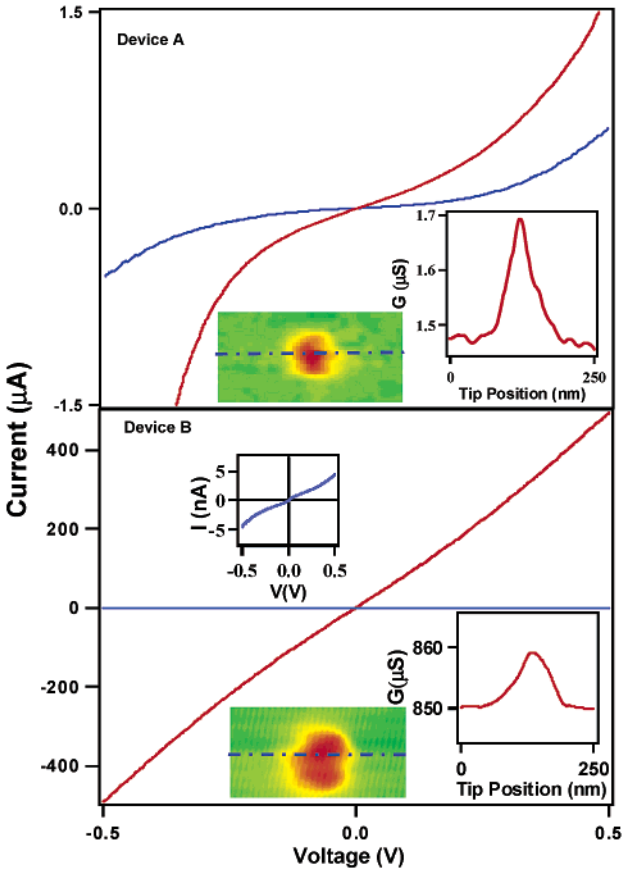

Figure 3. *I*−*V* characteristics of two different devices in their "off" (blue) and "on" (red) states, respectively (upper left inset for device B shows the *I*−*V* of the "off" state with an expanded scale). The insets in the lower-right quadrants show the color images of local conductance peaks at high magnification (color scale denotes conductance) and the line traces along the dotted lines.

The emergence of a nanoscale switching center is thus the signature of the junction switching to the "on" state.

Using the same technique, we then investigated the switching of a molecular device into its "off" state by following the evolution of an existing local conductance peak (Figure 4). Figure 4A shows the switching curve of a device that was switched off in two discrete steps. Figure 4B displays the line trace through a switching center at the initial, intermediate, and final states, where the pressure-induced conductance peak is reduced in magnitude with each switching step. After the device was switched into its final and lowest conductance state (blue curve in Figure 3A), the peak completely vanished and the conductance map was again uniform across the junction. Thus switching "off" the molecular junction is accompanied by the annihilation of a switching center.

In summary, under local mechanical pressure, a nanoscale conductance peak invariably appears when the device is switched "on", and disappears when switched "off". This observation constitutes our central experimental finding, demonstrating clearly that the conductance switching is related to the creation and annihilation of local inhomogenities in the device. The reversibility of the switching and the direct correlation of the change in device conductance with the

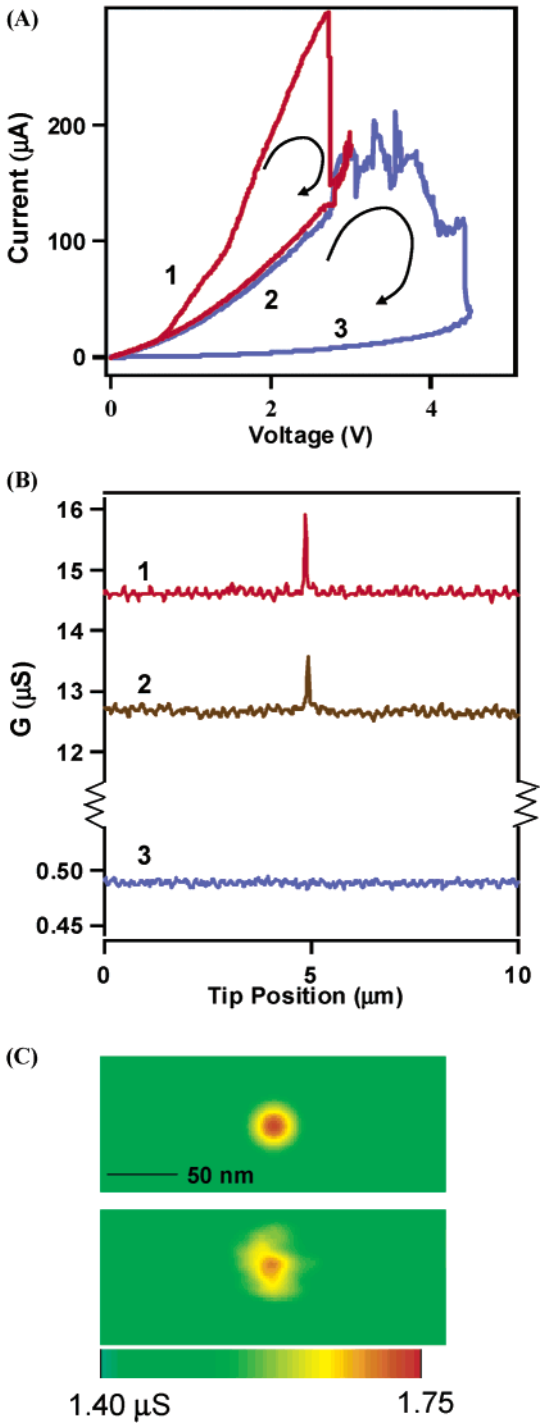

Figure 4. (A) Switching curve of a device, switched off in two discrete steps. The arrows indicate sweep direction, and the numbers 1, 2, and 3 denote the initial, intermediate, and final conductance state of the device, respectively. (B) Pressure-induced local conductance peak at each of the states. Note that the peak was reduced in magnitude with each switching step, and vanished completely in state 3. (C) Conductance as a function of tip position obtained from theoretical model calculated using eq 2 (top panel) and experimental data from device A (bottom panel).

emergence and disappearance of a nanoscale conductance peak leads us to conclude that these peaks are signatures of dominant conducting pathways, whose formation and destruction lead to the "on" and "off" state of a molecular switch device, respectively.

To understand this behavior we consider a simple model. In the "off" state the electrodes are uniformly separated by 26 Å, the molecular layer thickness. Transport through the molecular layers is by tunneling because stearic acids are electrical insulators. This is consistent with the high resistance observed in the "off" state. When the device is turned "on", we assume that within the nanoscale switching center the electrode spacing is smaller. Because of the exponential dependence of tunneling rate on distance, the conductance of the entire junction in the "on" state will be dominated by that of the small region. Thus, a conductance peak is observed only when the AFM tip is pressing this small region (nanoasperity) that dominates transport.

Quantitatively, we model the tunnel conductance of device A in the "on" state in response to applied pressure as

$$G_{on}(x, y) = (G_{on} - G_{off}) \exp(\alpha \delta z(x,y)) + G_{off} \qquad (2)$$

where the first term describes the tunneling conductance through the nanoasperity in response to local mechanical compression δz, α is the tunneling constant through alkane chains, and G_{on} and G_{off} are the unperturbed conductance of the junction in the "on" and "off" state, respectively. In the simulation, we take $G_{on} = 1.45\ \mu$S and $G_{off} = 0.17\mu$S as measured from the data, $\alpha = 1$ Å^{-1} as reported in the literature,[15] and $\delta z(x,y)$ is calculated from eq 1. Using eq 2, we calculate the conductance as a function of tip position (x,y), and the result (Figure 4C, left panel) reproduces the features observed in experimental data (right panel). Thus, our simple model, with no free parameters, readily accounts for the increased conductance in the "on" state, the presence of a conductance peak, and the pressure dependence of the peak height. Similar quantitative agreement between the model calculation and the experimental data was found for other samples with high "on" state resistance.

The presence of an asperity where the electrons tunnel through a relatively short distance in the on state suggests that switching to yet higher conductance states could lead to conductive filamentary pathways that bridge the electrodes entirely. We would expect in this case to see conductance on the order of the conductance quantum, $G_Q \sim 80\ \mu$S. This is indeed observed in device B: its conductance in the "on" state is $\sim 10\ G_Q$, and it shows a single switching center under applied force. The small pressure-enhanced conductance in this case likely results from small changes in contact resistance of the filament with the electrode or contributions from tunneling in parallel with the filament.

The high conductance observed in device B and the quantitative agreement between the model and the data in devices with high "on" state resistance strongly indicates that the switching behavior in our molecular structures results from the formation and dissolution of conducting filaments as the appropriate writing voltages are applied.

Further work will be required to fully elucidate the mechanisms of filament growth/dissolution, which may be electrochemical reaction,[20,21] thermal migration and/or electromigration.[22] Typically only a single switching center is observed, suggesting that the formation of a nanoasperity involves a runaway process of filament growth driven by increasing current density and/or electric field as the conductance increases. While filament formation may not be exclusive to devices with dissimilar electrodes, such devices have been essential for obtaining reversible switching in the samples we have studied to date. Thorough understanding of this switching mechanism may enable successful application of the unusually large on/off ratio ($\sim 10^5$) and nanometer scale of the switching centers to nanoscale memory and logic devices.

Acknowledgment. We thank P.A. Beck and D. Ohlberg for assistance with fabrication, and A. Bratkovski, B. Larade, and M. Tinkham for helpful discussion. This work was supported in part by DARPA(HP) and the Charles Lee Powell Foundation (M.B.).

References

(1) Ramachandran, G. K.; Hopson, T. J.; Rawlett, A. M.; Nagahara, L. A.; Primak, A.; Lindsay, S. M. *Science* **2003**, *300*, 1413.
(2) Gittins, D. I.; Bethell, D.; Schiffrin, D. J.; Nichols, R. J. *Science* **2000**, *408*, 67.
(3) Donhauser, Z. J.; Mantooth, B. A.; Kelly, K. F.; Bumm, L. A.; Monnell, J. D.; Stapleton, J. J.; Price, D. W.; Rawlett, A. M.; Allara, D. L.; Tour, J. M.; Weiss, P. S. *Science* **2001**, *292*, 2303−2307.
(4) Cui, X. D.; Primak, A.; Zarate, A.; Tomfohr, J.; Sankey, O. F.; Moore, A. L.; Moore, T. A.; Gust, D.; Harris, G.; Lindsay, S. M. *Science* **2001**, *294*, 571.
(5) Chen, J.; Wang, W.; Reed, M. A.; Rawlett, A. M.; Price, D. W.; Tour, J. M. *Appl. Phys. Lett.* **2000**, *77*, 1224−1226.
(6) Chen, J.; Reed, M. A.; Rawlett, A. M.; Tour, J. M. *Science* **1999**, *286*, 1550−1552.
(7) Collier, C. P.; Wong, E. W.; Belohradsky, M.; Raymo, F. M.; Stoddart, J. F.; Kuekes, P. J.; Williams, R. S.; Heath, J. R. *Science* **1999**, *285*, 391.
(8) Chen, Y.; Ohlberg, D. A. A.; Li, X.; Stewart, D. R.; Williams, R. S. *Appl. Phys. Lett.* **2003**, *82*, 1610.
(9) Chen, Y.; Jung, G.-Y.; Ohlberg, D. A. A.; Li, X.; Stewart, D. R.; Jeppesen, J. O.; Nielsen, K. A.; Stoddart, J. F.; Williams, R. S. *Nanotechnology* **2003**, *14*, 462.
(10) Stewart, D. R.; Ohlberg, D. A. A.; Beck, P. A.; Chen, Y.; Williams, R. S. *Nano Lett.* **2003**, in press.
(11) Collier, C. P.; Mattersteig, G.; Wong, E. W.; Luo, Y.; Beverly, K.; Sampaio, J.; Raymo, F. M.; Stoddart, J. F.; Heath, J. R. *Science* **2000**, *289*, 1172−1175.
(12) Rawlett, A. M.; Hopson, T. J.; Nagahara, L. A.; Tsui, R. K.; Ramachandran, G. K.; Lindsay, S. M. *Appl. Phys. Lett.* **2002**, *81*, 3043.
(13) Reed, M. A.; Chen, J.; Rawlett, A. M.; Price, D. W.; Tour, J. M. *Appl. Phys. Lett.* **2001**, *78*, 3735.
(14) Seminario, J. M.; Zacarias, A. G.; Tour, J. M. *J. Am. Chem. Soc.* **2000**, *122*, 3015.
(15) Wold, D. J.; Frisbie, C. D. *J. Am. Chem. Soc.* **2001**, *123*, 5549.
(16) Patrick, D. L.; Flanagan, J. F.; Kohl, P.; Lynden-Bell, R. M. *J. Am. Chem. Soc.* **2003**, *125*, 6762.
(17) Leng, Y.; Jiang, S. *J. Chem. Phys.* **2000**, *113*, 8800.
(18) Tutein, A. B.; Stuart, S. J.; Harrision, J. A. *J. Phys. Chem. B* **1999**, *103*, 11357−11365.
(19) Lifshitz, E. M.; Landau, L. D. *Theory of Elasticity*, 3rd ed.; Butterworth-Heinemann; London, 1959; Vol. 7.
(20) Terabe, K.; Nakayama, T.; Hasegawa, T.; Aono, M. *J. Appl. Phys.* **2002**, *91*, 10110−10114.
(21) Sakamoto, T.; Sunamura, H.; Kawaura, H.; Hasegawa, T.; Nakayama, T.; Aono, M. *Appl. Phys. Lett.* **2003**, *82*, 3032−3034.
(22) Ho, P. S.; Kwok, T. *Rep. Prog. Phys.* **1989**, *52*, 301.

NL035117A